

See discussions, stats, and author profiles for this publication at: <https://www.researchgate.net/publication/262562446>

In Situ Analysis of Bacterial Extracellular Polymeric Substances from a *Pseudomonas fluorescens* Biofilm by Combined Vibrational and Single Molecule Force Spectroscopies

ARTICLE *in* THE JOURNAL OF PHYSICAL CHEMISTRY B · MAY 2014

Impact Factor: 3.3 · DOI: 10.1021/jp5030872

CITATION

1

READS

42

5 AUTHORS, INCLUDING:



Fabienne Quilès

French National Centre for Scientific Research

38 PUBLICATIONS 563 CITATIONS

[SEE PROFILE](#)



Dima Jamal

Laboratoire de Chimie Physique et Microbiolo...

3 PUBLICATIONS 5 CITATIONS

[SEE PROFILE](#)



Grégory Francius

French National Centre for Scientific Research

66 PUBLICATIONS 1,282 CITATIONS

[SEE PROFILE](#)

In Situ Analysis of Bacterial Extracellular Polymeric Substances from a *Pseudomonas fluorescens* Biofilm by Combined Vibrational and Single Molecule Force Spectroscopies

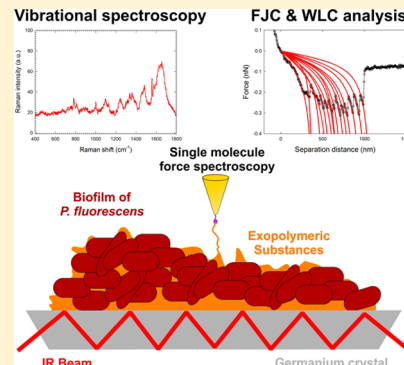
Ahmad Fahs,^{†,‡} Fabienne Quilès,^{†,‡} Dima Jamal,^{†,‡} François Humbert,^{†,‡} and Grégory Francius*,^{†,‡}

[†]Université de Lorraine, Laboratoire de Chimie Physique et Microbiologie pour l'Environnement, UMR 7564, Villers-lès-Nancy, F-54600, France

[‡]CNRS, Laboratoire de Chimie Physique et Microbiologie pour l'Environnement, UMR 7564, Villers-lès-Nancy, F-54600, France

S Supporting Information

ABSTRACT: Extracellular polymeric substances (EPS) play an important role in biofilm cohesion and adhesion to surfaces. EPS of a *P. fluorescens* biofilm were characterized through their vibrational spectra (infrared and Raman) and their conformational properties using single molecule force spectroscopy with specific probes for glucose, galactose, and *N*-acetyl glucosamine-rich EPS. Vibrational spectra evidenced the overproduction of glycogen and other carbohydrates in the biofilm. The conformational analysis was performed from both the freely jointed chain (FJC) and worm like chain (WLC) models. The results of the FJC fittings showed highly ramified and/or folded structures for all the detected EPS with molecular elongations up to 1000–2500 nm, and typical Kuhn lengths of glycogen macromolecules. The characteristics of galactose-rich EPS have been found to be significantly different from those of glucose- and *N*-acetyl glucosamine-rich EPS. On the basis of the theoretical fittings with the WLC model, our results suggested that carbohydrates may be associated with peptide domains.



INTRODUCTION

Bacteria synthesize functional molecules for intracellular uses, but they also produce extracellular polymeric substances (EPS). EPS have multiple functions and consist of polysaccharides, proteins, nucleic acids, and amphiphilic molecules. In addition to their relevance in cell aggregation, cohesion, and protective barriers of biofilms (i.e., a microbial sessile community with cells that are irreversibly attached to a surface), they play an essential role in bacterial adhesion to surfaces.¹ The bacterial adhesion depends on the intrinsic characteristics of the bacteria, the chemical and physical properties of the surface, and the environmental conditions.^{2,3} If the two last factors can be controlled during biofilm build-up, the complexity of the first one remains an obstacle to better understand the mechanisms of bacterial adhesion and biofilm formation. The physicochemical characterization of EPS constitutes a key study to explain such mechanisms, permitting more practical knowledge in biomedical, food, and pharmaceutical fields.^{2,4}

Previous works on EPS analysis, based on extraction and purification methods, have mentioned difficulties mostly related to membrane and cytoplasm components of bacteria.^{5,6} In agreement with different studies, the polysaccharides are a major fraction in EPS matrix,^{7,8} and play an indispensable role in colonization and biofilm formation.⁸ For *P. fluorescens* (*Pf*) strains, exopolysaccharides have been partly described as complex polymers containing monomers of sugars such as mannose, galactose, xylose, arabinose, and acetylated amino

glucoses.^{9–11} By combining the analysis of infrared fingerprints, specific staining of the bacteria, and single molecule force spectroscopy (SMFS) measurements, we have demonstrated the production of extracellular glycogen by planktonic *Pf* cells, and characterized it *in situ*, directly on live cells.¹² Infrared spectroscopy in attenuated total reflection mode (IR-ATR) is known to reach *in situ* information on the chemical composition of biofilms made of sessile bacteria.^{13,14} Another vibrational spectroscopy, Raman spectroscopy, is a non-destructive analytical technique, which enables spectral analysis with micrometer spatial resolution. It has proven to be suitable for the characterization of biological samples such as cells.^{15,16} Application to the study of fully hydrated biofilms is quite more recent.^{17–19}

Electron microscopy techniques,^{20,21} confocal laser microscopy,²² bioimmunochemical protocols,²³ and atomic force microscopy (AFM) are commonly used by the scientific community for the investigation of complex biological systems such as biofilms.²⁴ AFM demonstrated the possibility of realizing experiments, in a controlled environment, in order to show biofilm structure by imaging mode,^{25,26} and EPS conformational characteristics by force spectroscopic mode under wet or physiological conditions.²⁷ However, the

Received: March 28, 2014

Revised: May 21, 2014

Published: May 23, 2014

microscopic techniques alone cannot give all the chemical information such as a precise identification of the biomolecules constituting the biofilm matrix. The combination of microscopic and spectroscopic methods allows the complete analysis of the possible production of extracellular polysaccharides by sessile bacteria.

The aim of this work was to analyze *in situ*, directly on living cells, several EPS produced by *Pf* bacteria of a young biofilm using vibrational and single molecule force spectroscopies. For this, 21 h-old *Pf* biofilms have been formed in two flow cells at a moderately rich nutrient medium. The biofilm prepared on Ge crystal (compatible with both vibrational measurements) was characterized by IR-ATR and Raman spectroscopies and investigated at the nanoscale by AFM imaging. Using lectin-grafted AFM tips, specific EPS have been examined in terms of contour lengths, adhesion, and nanomechanical properties by SMFS, as a powerful technique for investigating biomolecular systems at the nanoscale level.

■ EXPERIMENTAL METHODS

Chemicals. Luria–Bertani (LB, Miller's) broth was purchased from Fluka. Glycogen from bovine liver (type IX, purity $\geq 85\%$), PBS pellets, sodium acetate, sodium maleate, $\{\text{MnCl}_2 \cdot 4 \text{ H}_2\text{O}\}$, $\{\text{CaCl}_2 \cdot 2 \text{ H}_2\text{O}\}$, lectin Concanavalin A (ConA), lectin from *Pseudomonas aeruginosa* (PAO1), and lectin wheat germ agglutinin (WGA) were purchased from Sigma-Aldrich (France). Sybr Green II and Concanavalin A labeled with Texas Red (ConA-Tx, Molecular Probes) was purchased from Invitrogen.

Bacterial Suspension for Biofilm Formation. *Pseudomonas fluorescens* CIP 69.13 was purchased from the collection of the Pasteur Institute (Paris, France). After a preculture for 24 h, *P. fluorescens* was cultured for 14 h in LB medium ($25 \text{ g} \cdot \text{L}^{-1}$) at $28 \pm 1^\circ\text{C}$ under magnetic stirring to reach the end of the exponential growth phase as described elsewhere.¹⁴ Bacteria were then harvested by centrifugation (8000 rpm, 10 min, 20 °C), and the pellet was resuspended in 200 mL of sterile 1:50 diluted LB medium ($0.5 \text{ g} \cdot \text{L}^{-1}$). The bacterial concentration was adjusted to an optical density of 0.28 at 620 nm (OD_{620}), which corresponds to approximately $10^8 \text{ CFU} \cdot \text{mL}^{-1}$. This suspension is hereafter called S0. OD_{620} was measured with a UNICAM Helios ε visible spectrophotometer.

Biofilm Formation. Biofilms were initiated in 1:50 diluted LB sterile medium ($0.5 \text{ g} \cdot \text{L}^{-1}$) in a flow cell containing a germanium crystal at 21°C in an air conditioned room.¹⁴ Briefly, bacterial suspension S0 was pumped into the flow cell for 3 h to promote bacterial adhesion. Then, the bacterial suspension was replaced by a sterile 1:50 diluted LB medium ($0.5 \text{ g} \cdot \text{L}^{-1}$) flow for the other 18 h, providing a biofilm aged of 21 h.

Flow Cells. To monitor the biofilm formation by infrared spectroscopy, an IR-ATR flow cell (SPECAC) enclosing a Ge crystal was used as described elsewhere.^{14,28} For the analysis of the 21 h-old biofilm by Raman spectroscopy and AFM, *Pf* biofilms were grown in a homemade flow cell. This flow cell consisted of a poly(methyl methacrylate) base plate that was milled out to form a shallow flow chamber and had an inlet and exit for liquid. Inside the flow chamber, there are places for two disks of Ge crystals. Using a gasket, a glass microscope plate was clamped on the top of the base to seal the flow cell. The advantage here was the possibility to record Raman spectra *in situ* as for infrared spectroscopy.

Infrared Spectroscopy. IR-ATR spectra were recorded *in situ* between 4000 and 800 cm^{-1} on a Bruker Vector 22 spectrometer equipped with a KBr beam splitter and deuterated triglycine sulfate (DTGS) thermal detector. The resolution of the single beam spectra was 4 cm^{-1} . Measurements were performed at $21 \pm 1^\circ\text{C}$ in an air-conditioned room. Water vapor subtraction and baseline correction (2 points at 1800 and 900 cm^{-1}) were performed. Recording of spectra, data storage, and data processing were performed using the Bruker OPUS 3.1. The number of bidirectional double-sided interferogram scans was 100, which corresponds to a 1 min accumulation. All interferograms were Fourier processed using the Mertz phase correction mode and a Blackman–Harris three-term apodization function. No ATR correction was performed. IR-ATR spectra are shown with an absorbance scale corresponding to $\log(R_{\text{reference}}/R_{\text{sample}})$, where R is the internal reflectance of the device. In the course of biofilm monitoring experiments, IR-ATR spectra were recorded every 10 or 15 min.

Raman Spectroscopy. Raman spectra were collected in the range 400 – 1800 cm^{-1} with a Jobin-Yvon ISA T64000 spectrometer equipped with an Olympus BX41 confocal microscope. Measurements were recorded using an Olympus $\times 50$ objective and a confocal pinhole of $200 \mu\text{m}$. The instrument was equipped with an edge filter to eliminate the Rayleigh scattering, 1200 grooves per millimeter grating, and a charge coupled device (CCD) working at low temperature (140 K) with a 1024 by 256 pixels array. The excitation source was an ionized argon laser at 488 nm, generating $\sim 20 \text{ mW}$ on the sample, to avoid thermal degradation. The biofilm of *Pf* was analyzed *in situ* directly in the flow cell by setting the flow cell under the microscope objective. For comparison, planktonic *Pf* cells at end-exponential phase were analyzed by depositing on a germanium disk a pellet harvested by centrifugation (8000 rpm, 10 min, and 20°C) after 14 h of culture in LB medium at $25 \text{ g} \cdot \text{L}^{-1}$. The acquisition time was 12 min per spectrum, and all data were imported to LabSpec5 and Origin software's for treatment.

Epifluorescence Optical Microscopy and Immuno-Staining. Biofilm of *Pf* was stained with lectin Concanavalin A–Texas Red (ConA-Tx) that links with glucosyl and mannosyl residues. The Ge crystal was carefully removed from the flow cell, rinsed with nonpyrogenic sterile water to remove nonadherent cells, and stained with a solution of ConA-Tx (0.5 g/L in Tris–maleic buffer, beforehand centrifuged at 9000 rpm for 10 min to remove aggregates) for 20 min in the dark. The Ge crystal was then rinsed with nonpyrogenic sterile water to eliminate excess ConA-Tx and wicked dry with filter paper to remove excess water. The sample was visualized with an Olympus BX51 microscope using immersion oil $\times 100$ objectives and equipped with an Olympus XC50 camera.

Chemical Immobilization of Lectins on the AFM Tip. In order to probe specific interactions with cell surface polysaccharides using SMFS, AFM tips were chemically modified by three types of lectin. Lectins ConA, PAO1, and WGA were separately used to specifically detect polysaccharide molecules containing glucose and mannose, galactose, and *N*-acetyl glucosamine, respectively. Silicon nitride cantilevers of square pyramidal shape tip (radius of curvature $\sim 20 \text{ nm}$) were purchased from Bruker (MLCT-Au, Bruker Nano AXS, Palaiseau, France). AFM tips were functionalized with the lectins via a 6 nm-long poly(ethylene glycol) linker, according to the protocol published by Hinterdofer et al.²⁹ and Francius et al.³⁰

Atomic Force Microscopy and Single Molecule Force Spectroscopy (SMFS) Experiments. AFM and SMFS experiments were carried out using an MFP3D-BIO instrument (Asylum Research Technology, Atomic Force F&E GmbH, Mannheim, Germany). Topographical images of the biofilms were performed by contact mode AFM in PBS buffer solution (pH 7.2). In order to avoid any damage during imaging, we used nonfunctionalized MLCT-Au cantilevers (Bruker Nano AXS, Palaiseau, France) having a low spring constant of 10–15 pN/nm. Note that the applied force between the tip and the surface was carefully monitored and minimized below 250 pN. Under these conditions, the effect of mechanical damage of the biofilm was prevented, and good AFM images can be obtained. All images were collected with a resolution of 512 × 512 pixels and a scan rate of 1 Hz. For the single molecule force spectroscopy (SMFS) experiments, the force/volume mode was used to record the force–displacement curves. SMFS measurements were obtained by recording a grid map of 32 × 32 force–displacement curves at three different locations of the biofilm surface corresponding to a scan area of 30 μm × 30 μm. Experiments were performed using a constant approach and retraction speed of 6000 nm/s and a maximum applied force of 500 pN. The spring constants of cantilevers (k_c) were determined using the thermal calibration method, providing k_c values in the range 10–15 pN/nm. Interaction forces (F) are calculated following Hooke's law:

$$F = k_c \cdot \Delta d \quad (1)$$

where Δd (nm) is the cantilever deflection.

When an AFM probe is functionalized by a lectin, the rupture events occurring in the SMFS experiments correspond to the stretching of the polysaccharide-based macromolecules (except for the last rupture event which corresponds to the complete detachment from the tip, all of them correspond to the unfolding of the macromolecule). Force–displacement curves were analyzed on the formalism of the freely jointed chain (FJC) and the worm like chain (WLC) models.^{31,32} Briefly, the FJC model describes macromolecules consisting of rigid segments that are free to rotate around their connections. It predicts that the mean extension z under constant force F follows a Langevin function:³¹

$$z(F) = -L_c \left[\coth \left(\frac{FL_k}{k_B T} \right) - \frac{k_B T}{FL_k} \right] \quad (2)$$

where the Kuhn length l_k is a direct measure of the chain stiffness, L_c is the total contour length of the macromolecule, k_B is the Boltzmann constant, and T is the temperature.

Within the framework of the WLC model, it is assumed that the macromolecule consists of an irregular curved filament, which is linear on the scale of the persistence length l_p . The pulling force F may then be expressed as a function of z , the macromolecule extension via the expression^{31,33}

$$F(z) = -\frac{k_B T}{l_p} \left[\frac{1}{4} \left(1 - \frac{z}{L_c} \right)^{-2} + \frac{z}{L_c} - \frac{1}{4} \right] \quad (3)$$

where L_c is the total contour length of the macromolecule, k_B is the Boltzmann constant, T is the temperature, and l_p is the persistence length.

The choice of the most suitable model was determined by the best fitting quality parameter, q_{min} , calculated by eq 4:

$$q_{min} = \min \left(\sum_{i=0}^n \left[\left(1 - \frac{F_{\text{calc}}(i)}{F_{\text{exp}}(i)} \right)^2 \right]^{1/2} + \sum_{i=0}^n \left[\left(1 - \frac{z_{\text{calc}}(i)}{z_{\text{exp}}(i)} \right)^2 \right]^{1/2} \right) \quad (4)$$

where n is the number of points in an experimental segmented force curve, $F_{\text{exp}}(i)$ and $z_{\text{exp}}(i)$ are the experimental data at point i , and $F_{\text{calc}}(i)$ and $z_{\text{calc}}(i)$ are the calculated values obtained from the theoretical models at point i . q_{min} was calculated at each rupture after segmentation (see more details in Polyakov et al.³⁴).

RESULTS AND DISCUSSION

Vibrational Analysis of the 21 h-old *P. fluorescens* Biofilm. Figure 1 shows the vibrational spectra of sessile (IR-ATR (Figure 1a) and Raman (Figure 1b)) and planktonic (Raman, Figure 1b) *Pf* bacteria of this study. The Raman spectra were recorded with an excitation wavelength of 488 nm to avoid the Raman resonance effect of cytochrome *c* that occurs in *Pf* cells.^{35,36} The IR-ATR spectra were characteristic of *Pf*.^{12,14} The fingerprint of the main components of the bacteria occurred in the IR-ATR spectrum: proteins, nucleic acids, and carbohydrates (Figure 1a). As it was already observed for some planktonic *Pf* grown in the same nutritive medium, a weak production of glycogen can also be observed here.¹² Indeed, bands at 1153 and 1024 cm⁻¹ can be observed in the spectrum of the 21 h-old biofilm, and they are highlighted in the second derivative spectra of the region of interest inserted in Figure 1a. These bands were not present in the spectra of the 3 h-old biofilm where no significant EPS production occurred.¹⁴ ConA-Tx does not penetrate into the cells, and it was used to probe the occurrence of extracellular glucose-rich polymers. The epifluorescence images show discontinuous fluorescent regions rather localized on the periphery of the bacteria (Figure 1a). It can be suggested that at least a part of the produced glycogen was extracellular. The *in situ* chemical signature of the *Pf* biofilm grown on a germanium crystal was also recorded by Raman microspectroscopy. In order to better investigate the Raman spectrum of the *Pf* biofilm, we have also examined that of bacteria harvested at the end-exponential growth phase.

Figure 1b shows the spectrum of planktonic bacteria at the end-exponential phase and of their sessile counterparts in the fully hydrated 21 h-old biofilm. Tentative assignments of the main bands were made in accordance with the literature,^{18,37,38} and they are given in Figure 1b. The spectra were normalized to the amide III band (1190–1280 cm⁻¹, Figure 1b), which represents the protein content. The latter does not vary significantly in bacteria, and it is often chosen as an indicator of biomass accumulation.³⁹ Raman spectroscopy is sensitive to the bacterial growth phase,¹⁶ and to physiological variations in the bacteria.⁴⁰ The spectra of both sessile and planktonic bacteria showed bands corresponding to the main components of bacterial cells (Figure 1b). However, several differences related to the proportions of cellular components were noticed. The amount of nucleic acids (782 and 1483 cm⁻¹) with respect to proteins (amide III band ~1240 cm⁻¹) was higher for sessile bacteria with respect to planktonic bacteria at the end-exponential phase. The higher production of nucleic acids

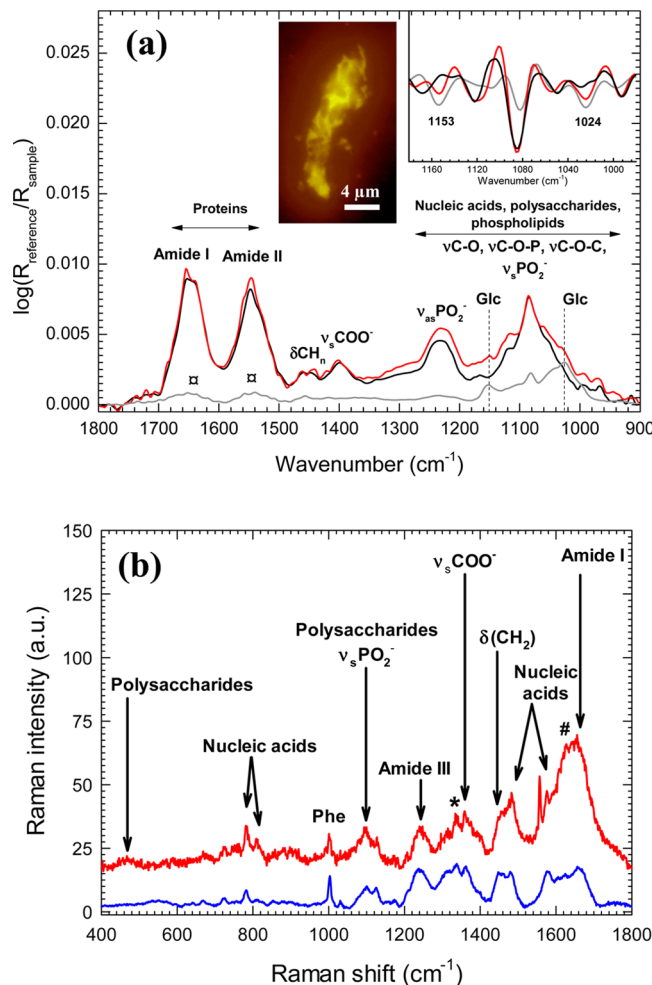


Figure 1. (a) IR-ATR spectra of glycogen (1.25 g/L in water, gray spectrum) and the 3 h-old (black spectrum) and 21 h-old (red spectrum) *P. fluorescens* biofilms. Spectra of biofilms are normalized with respect to the band near 1080 cm⁻¹. Insets: epifluorescence image of the 21 h-old biofilm stained with ConA-Texas red and second derivative spectra in region 1180–980 cm⁻¹. (b) Raman spectra of planktonic bacteria (bottom) and sessile bacteria in the 21 h-old biofilm (upper) recorded at an excitation wavelength of 488 nm. Key: δ , bending; ν , stretching; s , symmetric; as , antisymmetric; Glc, glycogen; \square , proteins in the commercial sample of glycogen; *, $\delta(CH)$; #, $\delta(H_2O)$.

suggested a higher metabolic activity in the biofilm. Likewise, the carbohydrate amount (~ 570 and 1050–1150 cm⁻¹) with respect to proteins (amide III band) was also higher for the bacteria in the biofilm as compared to that of planktonic bacteria at the end-exponential phase. This carbohydrate production may be assigned to a high production of polysaccharide-rich EPS within the biofilm. Unfortunately, it was not possible to identify the occurrence of glycogen or other specific polysaccharides (as galactan or poly-N-acetyl glucosamine, see Figure S1 in the Supporting Information) in the recorded Raman spectra. This strongly suggested that the polysaccharides produced by sessile *Pf* consisted of a mixture of several carbohydrates.

Morphology of the 21 h-old *P. fluorescens* Biofilm. After biofilm growth, the germanium surfaces were gently rinsed with a PBS buffer solution and immediately used for AFM analysis. Figure 2 presents two AFM topographical images of the *Pf* biofilm at two different scales (50 × 50 μm²

and 20 × 20 μm²). The AFM images showed a dense coverage by the bacteria that were maintained after the rinse. These good adhesion properties are a key feature that has to be ensured before single molecule force spectroscopy experiments.

The height profiles, given below each image, evidenced the presence of important depth differences of about 300–500 nm and smaller ones of about 50–150 nm. Considering the bacterial diameter is around 600–700 nm, the differences observed in height profiles along the cross section indicated the heterogeneous spatial organization of the biofilm, which was composed of mono- and also multilayers of bacteria. This result is in accordance with the observations made by epifluorescence microscopy.⁴¹ Besides, sessile *Pf* were longer with respect to planktonic bacteria with a size of about 2.5 μm long instead of 1–2 μm.¹² The rms (root-mean-square) roughness of the biofilm was about 160 nm. This value is about 4–6-fold lower than the bacterial diameter; this reflects the high coverage of the Ge surface, and probably the occurrence of a multilayered biofilm. Indeed, the mean surface coverage of the 21 h-old biofilm, evaluated on six different AFM images (30 × 30, 40 × 40 and 50 × 50 μm² sizes), was about 95% (data not shown). Besides, epifluorescence microscopy (Sybr Green II staining) also showed a high covered surface with a mean value of 70% evaluated on 38 images (90 × 65 μm² size, data not shown). The present result shows the ability of *Pf* to highly cover the Ge surface. The EPS cannot be imaged in aqueous media by contact mode AFM because their structures are too soft and mobile. However, their occurrence can be suggested on the images that are blurred, and resulted from the AFM tip stuck into the biofilm.

Evidence of the Occurrence of Extracellular Glycogen by SMFS. The occurrence of glycogen in this 21 h-old biofilm was formally identified by infrared spectroscopy. The immunostaining with fluorescent ConA-Tx proved that at least a part of the glycogen was extracellular (Figure 1a). The use of functionalized AFM probes specific to glucose and mannose allows the detection or location of the macromolecules and then the study of their conformational properties. Figure 3a,b shows a typical experimental force curve (retraction phase) recorded on the 21 h-old *Pf* biofilm using ConA functionalized AFM tips. The force curves recorded on the *Pf* biofilm generally possess a high peak force at the beginning of the curve, which is attributed to several interactions between the tip and the cell wall of bacteria.

This peak is followed by a sawtooth pattern due to the extension of the EPS chains. The analysis of the force curves revealed that most molecular elongations occurred until 1200–1500 nm of separation distance. Theoretical fittings performed with the FJC model (red lines in Figure 3a,b) exhibited a general fit with good quality. Besides, the quality of the theoretical fittings would be improved by using another more suitable model. For that, the whole force curves were also analyzed with the WLC model (blue lines in Figure 3a,b). To determine the proportion of the best fits of rupture events for each model, the fitting quality parameter qmin (defined in the Experimental Methods section) was used as a criterion (the lower the qmin, the better the fit). Figure 4a shows the statistical distribution of optimization parameters (qmin) for FJC and WLC fits using the ConA tip. The frequency of low qmin values (<0.002) was significantly higher for the FJC model with respect to the WLC model. This result was confirmed by the best fitting distribution obtained on 4096 force curves (Figure 4b). Indeed, 75% of the whole rupture

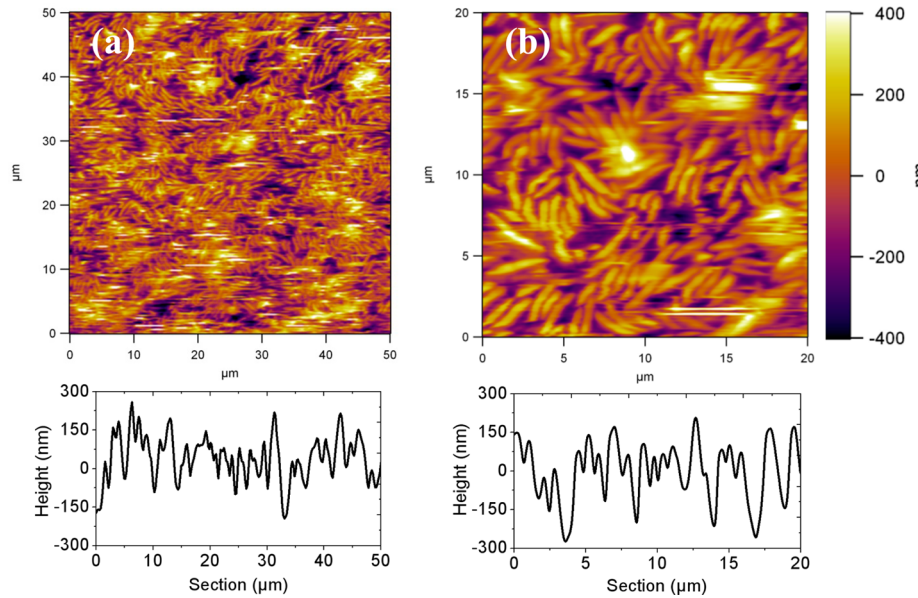


Figure 2. AFM topographic images of the 21 h-old biofilm of *P. fluorescens* at two different scales: $50 \times 50 \mu\text{m}^2$ (a) and $20 \times 20 \mu\text{m}^2$ (b). Imaging has been performed in PBS buffer solution (pH 7.2) by using contact mode AFM. The vertical scale bar is 800 nm.

events were best fitted by FJC, whereas only less than 20% were better fitted by WLC. This is another proof, in accordance with the infrared result, that glucose-rich polysaccharide (i.e., glycogen here) was overproduced in the 21 h-old biofilm.

Figure 5 reports the statistical distribution of the conformational properties obtained with both models. Seven conformational parameters were examined: the number of rupture peaks (i.e., the number of rupture events in the retraction force curves), contour length L_c , Kuhn length l_K (FJC model), last rupture length L_{\max} , persistence length l_p (WLC model), distribution of adhesion forces (i.e., the difference between the baseline and the last peak in the retraction force curve), and distance δL between two consecutive rupture events (see Figure S2a in the Supporting Information). We note that conformational parameters such as the contour length, rupture forces, periodicity, and number of ruptures per force curve remained the same for FJC and WLC models. Figure 5a shows that glucose/mannose-rich EPS can be detected onto 50% of the total surface of the explored biofilm.

This value was calculated from the percentage of pixels without any adhesive or rupture events. Hence, a significant number of retraction force curves showed rupture events, as a result of the presence of EPS rich in glucose/mannose residues on biofilm. A broad distribution of the number of rupture events per force curve was counted with most frequent values in the range of 10–16 ruptures (Figure 5a). In addition, the statistical analysis of the contour lengths showed a broad asymmetrical distribution ranging from 50 up to 2000 nm, with the most frequent L_c values around 500 nm (Figure 5b). The statistical distribution of l_K also showed a broad distribution with one maximum at about $l_K \sim 0.07$ nm and a broad distribution ranging from 0.15 up to 0.90 nm (Figure 5c). The value of 0.07 nm corresponds to the elongation of a single sugar molecule following a conformational change of a C5–C6 bond position.^{32,42} Even though some Kuhn length values were smaller than the one for the individual sugar ring, the literature provides examples of such values for polysaccharides and glycoproteins obtained by SMFS.^{43,44} The distribution of last rupture distance L_{\max} (Figure 5d) showed a Gaussian shape

distribution centered around 1200 nm. This is twice the most frequent L_c value (Figure 5b). The fact that L_{\max} is significantly higher suggested that either the macromolecules are linear but highly folded and/or branched. Since glycogen was formally identified by infrared spectroscopy, the second hypothesis is more probable due to the known ramified structure of glycogen.⁴⁵ The distribution of persistence lengths l_p calculated with the WLC model also showed a broad distribution ranging from 0.02 to 0.70 nm with one maximum near 0.06 nm. This value could be related to weak deformations of the turns inside the helical structures.^{46,47} The other values can be related to the typical pitch distances for α - and β -helices, and also to amino acid sizes that are in the range 0.15–1.20 nm.^{48–50} This result suggests the possible occurrence of some peptide domains within the glucose-rich EPS.

The statistical analysis of the amplitudes of the last rupture forces reported in Figure 5f revealed two maxima at about 50 and 80–90 pN. The first value is the most frequent, and it can be attributed to a single molecule interaction in accordance with experiments performed on glucose model surfaces.³⁰ The magnitude of the second maximum of adhesion forces is proportional to the number of glucose-rich macromolecules simultaneously interacting with the tip during retraction, i.e., about two. Here, it is emphasized that WLC and FJC analyses are valid because of single molecule interactions. The periodicity of rupture distances δL showed an asymmetric distribution centered around 50 nm (see Figure S2a in the Supporting Information) in the biofilm in contrast to a multimodal distribution of 30, 60, 90, and 120 nm for planktonic bacteria grown during 21 h in the same 1:50 diluted LB medium.¹² This difference suggests a loss in glycogen periodicity, and probably a lengthening of its branches in the 21 h-old biofilm. Thus, the results obtained for this biofilm show that the metabolism of the bacteria in biofilm lifestyle favors the production of polymers with longer chains at the expense of regular branches.

Detection and Conformational Analysis of Other Exopolymeric Substances by SMFS. Whereas our IR-ATR spectra have identified in an incontestable way the occurrence

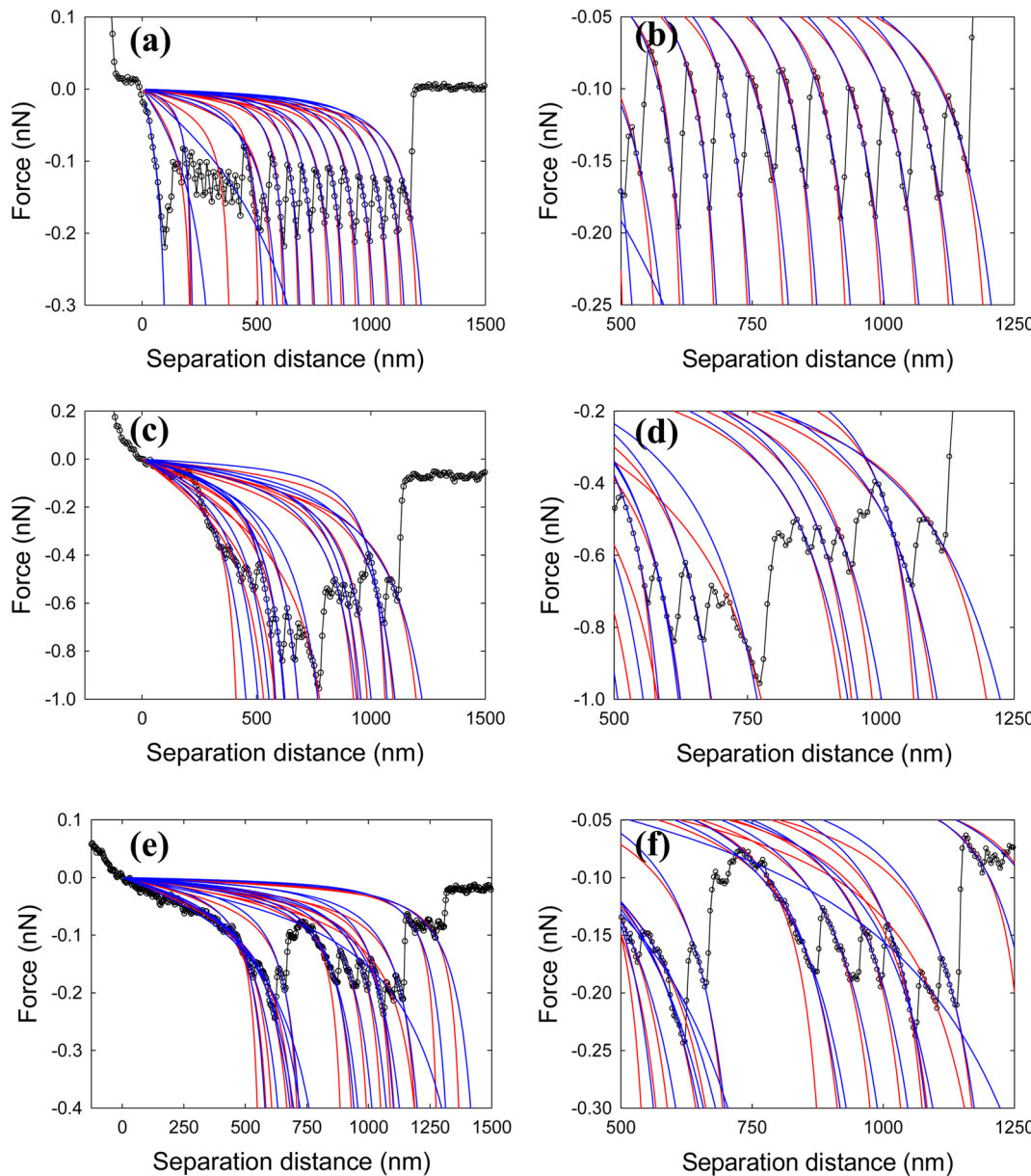


Figure 3. Representative experimental force–displacement curves (retraction phase, open circles) performed by SMFS on the 21 h-old *P. fluorescens* biofilm using (a, b) the Concanavalin A functionalized AFM tip, (c, d) the PAO1 functionalized AFM tip, and (e, f) the WGA functionalized AFM tip. Parts b, d, and f correspond to a zoom of the complete retraction force curve reported in parts a, c, and e, respectively. FJC (red lines) and WLC fittings (blue lines) are also shown.

of glycogen, the SMFS technique allowed the detection and the distribution of this glycogen on almost the entire analyzed surface. Raman spectra showed the overproduction of other polysaccharides in the 21 h-old biofilm. Thus, we used other lectins grafted to the AFM tips to detect and characterize potential EPS rich in galactose and N-acetyl glucosamine using PAO1 and WGA lectins, respectively. The 21 h-old *Pf* biofilm was investigated over a 30 μm by 30 μm area with the force–volume mode. Typical force curves showing the detected EPS are reported in Figure 3c–f, and the statistical analysis of conformational properties of these macromolecules is also shown in Figures 6 and 7. For the experiments performed with PAO1 and WGA AFM tips, the force curves were analyzed with FJC and WLC models. As for experiments made with ConA lectin, theoretical fittings performed with the FJC model were not completely in good agreement with the experimental curves

(Figure 3d,f). A significant number of retraction peaks were better fitted with the WLC model (Figure 4). Indeed, the statistical distributions of q_{\min} for both models were not significantly different in frequency and in absolute values (Figure 4c,e). Regarding the fittings with the FJC model, the proportion of the best fits of rupture events was only about 50% for PAO1 and WGA (Figure 4d,f). These results indicated that the detected EPS were very complex and probably contained peptide domains. Besides, these results are consistent with the Raman spectrum of the biofilm (Figure 1b). Of note, Raman results showed an overproduction of polysaccharides, but no formal identification was possible. This can be explained by the fact that the polysaccharide chains were not long enough, and/or the macromolecules were associated with peptide domains.

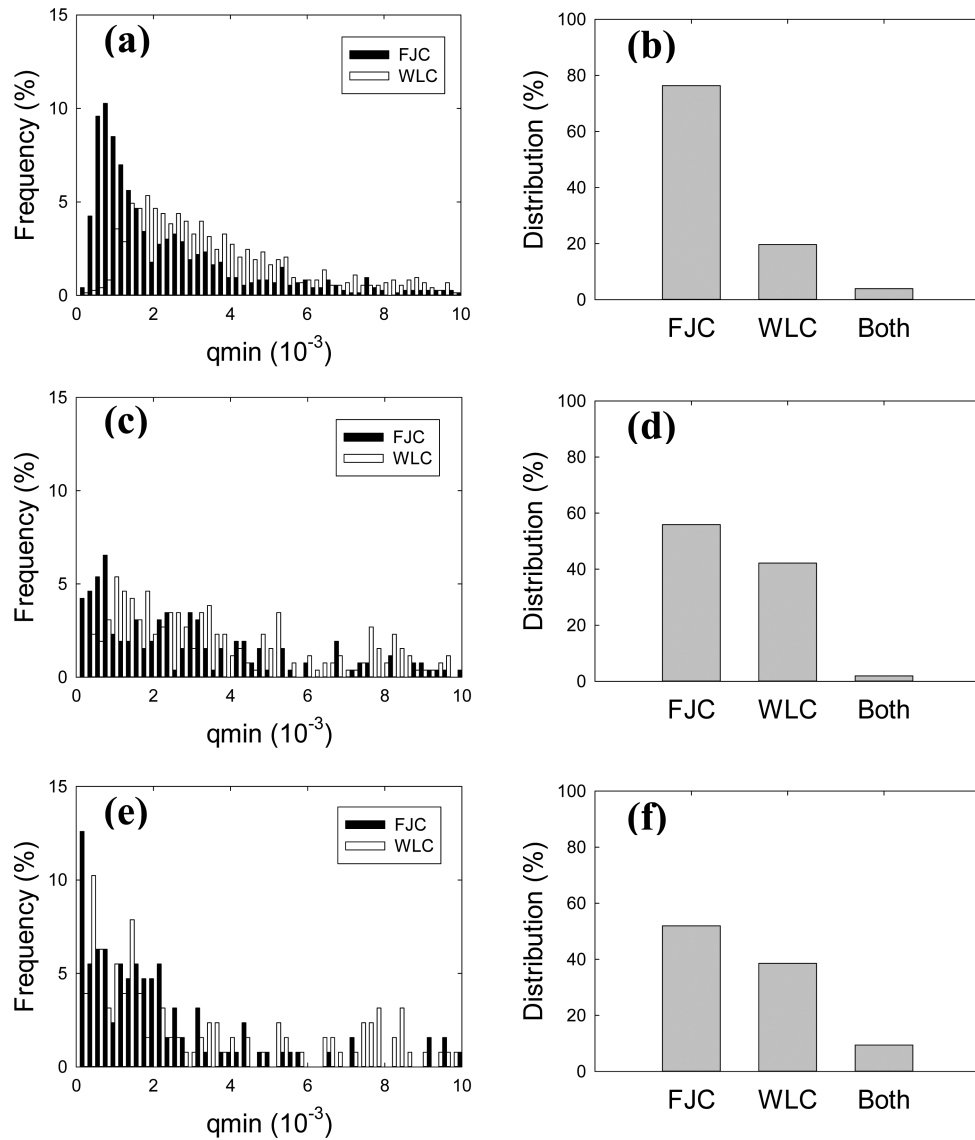


Figure 4. Comparison of the quality of the FJC and WLC fittings. (a, c, e) Statistical distribution of optimization parameters (q_{min}) of the force curve fittings by FJC and WLC models from Concanavalin A, PAO1, and WGA modified tips, respectively. (b, d, f) Best fitting distribution for FJC and WLC models for experiments performed with ConA, PAO1, and WGA-grafted AFM tips, respectively. When the difference of the fitting quality is not significant (<5%), the corresponding curves are assigned to “both” models agreement. Otherwise, the curves are assigned to models FJC or WLC as a function of the lower q_{min} .

In-depth analysis of the force curves allowed identifying the conformational characteristics of these galactose- and N-acetyl glucosamine-rich EPS. Figures 6 and 7 show the statistical distributions of the conformational parameters calculated from the FJC and WLC models. Exopolymers rich in galactose and N-acetyl glucosamine were respectively detected onto about 65% (Figure 6a) and 40% (Figure 7a) of the total surface of the biofilm (values calculated from the percentage of pixels without any rupture events). As observed for the ConA experiments, broad statistical distributions of the number of rupture events per force curve ranged from 5 to 15 ruptures in the case of PAO1 (Figure 6a) and from 1 to 15 ruptures in the case of WGA (Figure 7a). The contour lengths also showed broad asymmetrical distributions ranging from 50 up to 3000 nm, with the most frequent L_c values between 100 and 1000 nm (Figures 6b and 7b).

Whereas the statistical distribution of l_K showed a pronounced peak at about 0.05 nm for PAO1 experiments (Figure 6c), a broad and asymmetric distribution in the range 0.04–1.00 nm was calculated for WGA experiments (Figure 7c). The value of 0.05 nm is close to that of the elongation of a single sugar molecule following a conformational change of a C5–C6 bond position.^{32,42} For the PAO1 experiments, the distribution of the last rupture distance L_{max} showed a broad bell-shape distribution centered around 2200 nm (Figure 6d). This was about 10-fold of the most frequent L_c value (Figure 6b). This again suggested that the macromolecules are highly folded, and/or branched. The distribution of the last rupture distance L_{max} for the WGA experiments (Figure 7d) was different from that of PAO1 experiments. It showed a bimodal distribution with one pronounced Gaussian centered around 1000 nm. This was in the same order of the most frequent L_c value, indicating that these EPS were less folded and/or

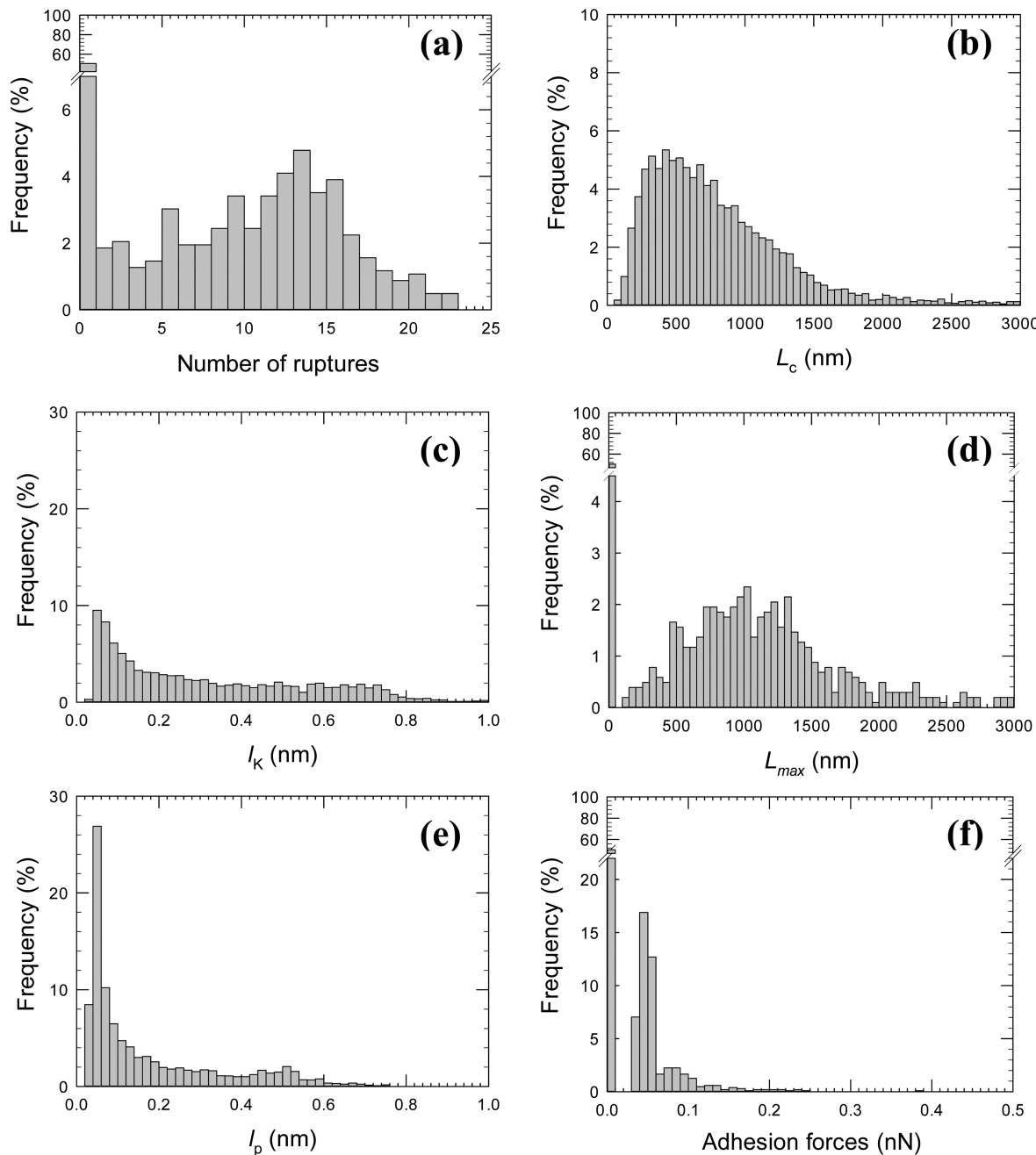


Figure 5. Conformational properties of glucose-rich EPS of *P. fluorescens* 21 h-old biofilm obtained by single molecule force spectroscopy (SMFS) by using a ConA functionalized AFM tip. Statistical distributions of (a) the number of ruptures, (b) contour length L_c , (c) Kuhn length l_K , (d) maximum length of the retraction curve L_{\max} , (e) persistence length l_p , and (f) the adhesion forces (i.e., the force at the last rupture).

branched. The distributions of persistence lengths l_p calculated with the WLC model for both lectins showed the same features with a broad distribution ranging from 0.02 to 0.80 nm with one maximum near 0.04–0.07 nm. This low value could also be associated with the weak deformations of the turns inside helical structures.^{46,47} These results reinforced the hypothesis of a possible occurrence of peptide domains in the galactose- and *N*-acetyl glucosamine-rich EPS, as it was also suggested above in the glucose-rich EPS.

Concerning the distributions of the last rupture force (or adhesion), the statistical analysis showed interactions in the same range (from 20 to 150 pN) for both galactose- and *N*-acetyl glucosamine-rich EPS (Figures 6f and 7f) with respect to poly-glucose. Both distributions clearly exhibited a maximum

around 50 pN, which equally corresponded to single molecule adhesions on model reference surfaces. The higher adhesion force values remained under 150 pN, resulting from simultaneous detachment of three macromolecules at maximum. In addition, when comparing the L_{\max} and the δL distributions for each lectin, analogous distributions for ConA and WGA experiments can be observed. EPS containing glucose and *N*-acetyl glucosamine sugars might exhibit close structures. Conversely, the distributions from the PAO1 experiment showed a twice lower most frequent value for δL (~25 nm) and a twice higher most frequent value for L_{\max} (~2200 nm). This underlined that galactose-rich EPS exhibited a significantly different structure with respect to the two other investigated EPS. For the three lectins used, the rupture events

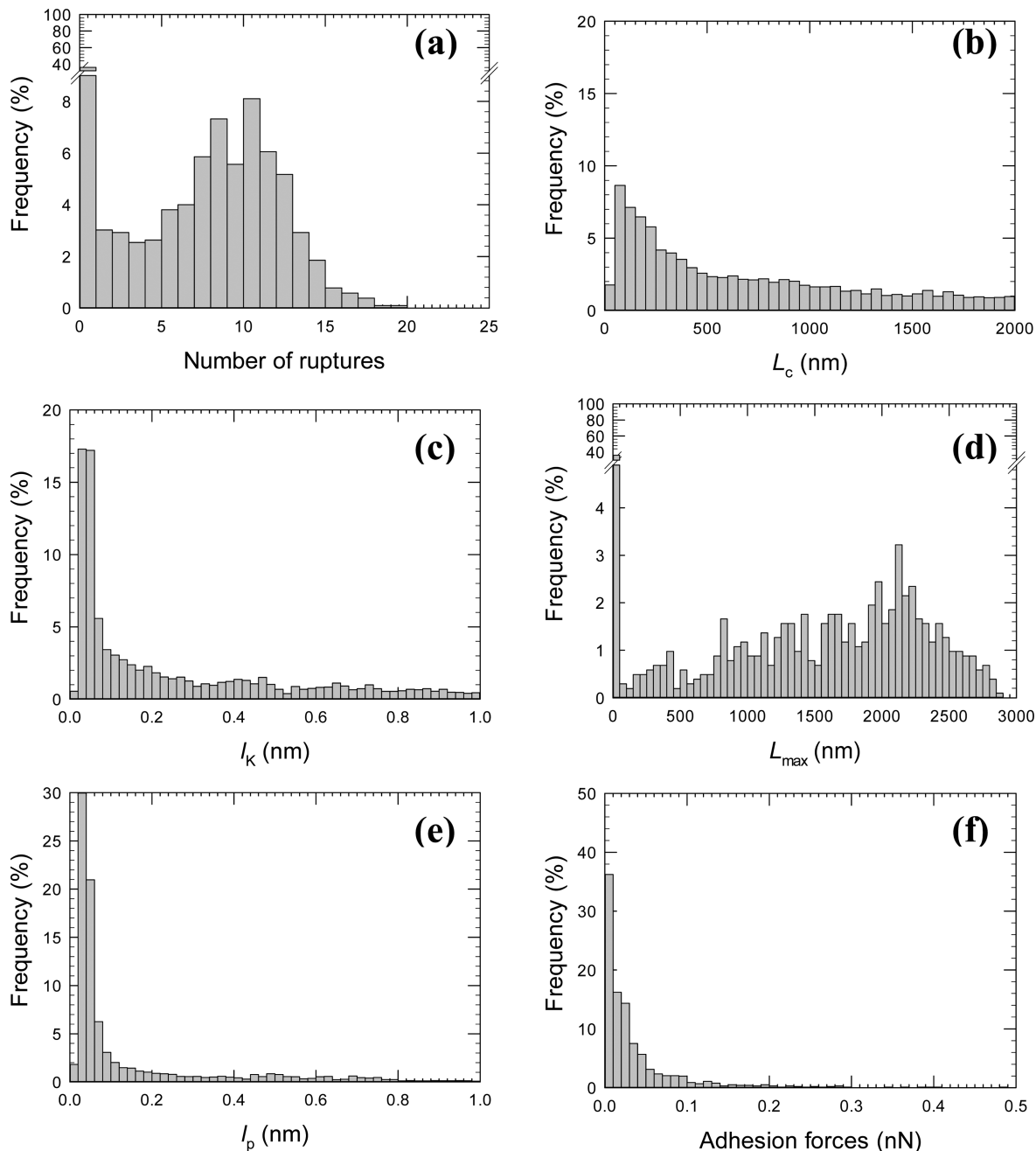


Figure 6. Conformational properties of poly-galactose-rich EPS of *P. fluorescens* 21 h-old biofilm obtained by single molecule force spectroscopy (SMFS) by using a PAO1 functionalized AFM tip. Statistical distributions of (a) the number of ruptures, (b) contour length L_c , (c) Kuhn length l_K , (d) maximum length of the retraction curve L_{max} , (e) persistence length l_p , and (f) the adhesion forces (i.e., the force at the last rupture).

were more or less well fitted by the FJC and WLC models. These models are usually considered suitable for the description of the mechanical behavior of polysaccharides and polypeptides under molecular stretching, respectively. Whereas the specific lectin probes only allow the binding to specific sugar, the occurrence of peptide domains within the polysaccharide main chain was evidenced by the WLC model. Comparing Figure 4b with Figure 4d,f, one can consider that the proportion of peptide domains was higher in galactose- and *N*-acetyl glucosamine-rich EPS with respect to glucose-rich EPS. Our results showed that *Pf* can produce and release very complex EPS as oligopolysaccharides and proteoglycans or glycoproteins with an important diversity in terms of structure.

CONCLUSION

In this study, we have characterized several EPS of a *P. fluorescens* biofilm grown on a Ge surface *in situ*. The combination of vibrational spectroscopies and the single molecule force technique provided complementary information about the structural and conformational properties of the EPS of the bacterial biofilm. Whereas infrared spectroscopy only showed the occurrence of glycogen, Raman spectroscopy allowed us to locally detect other carbohydrates for sessile bacteria. Interestingly, SMFS experiments performed using three carbohydrate-specific probes evidenced the additional occurrence of galactose and *N*-acetyl glucosamine-rich EPS. Conformational properties of the EPS were investigated from

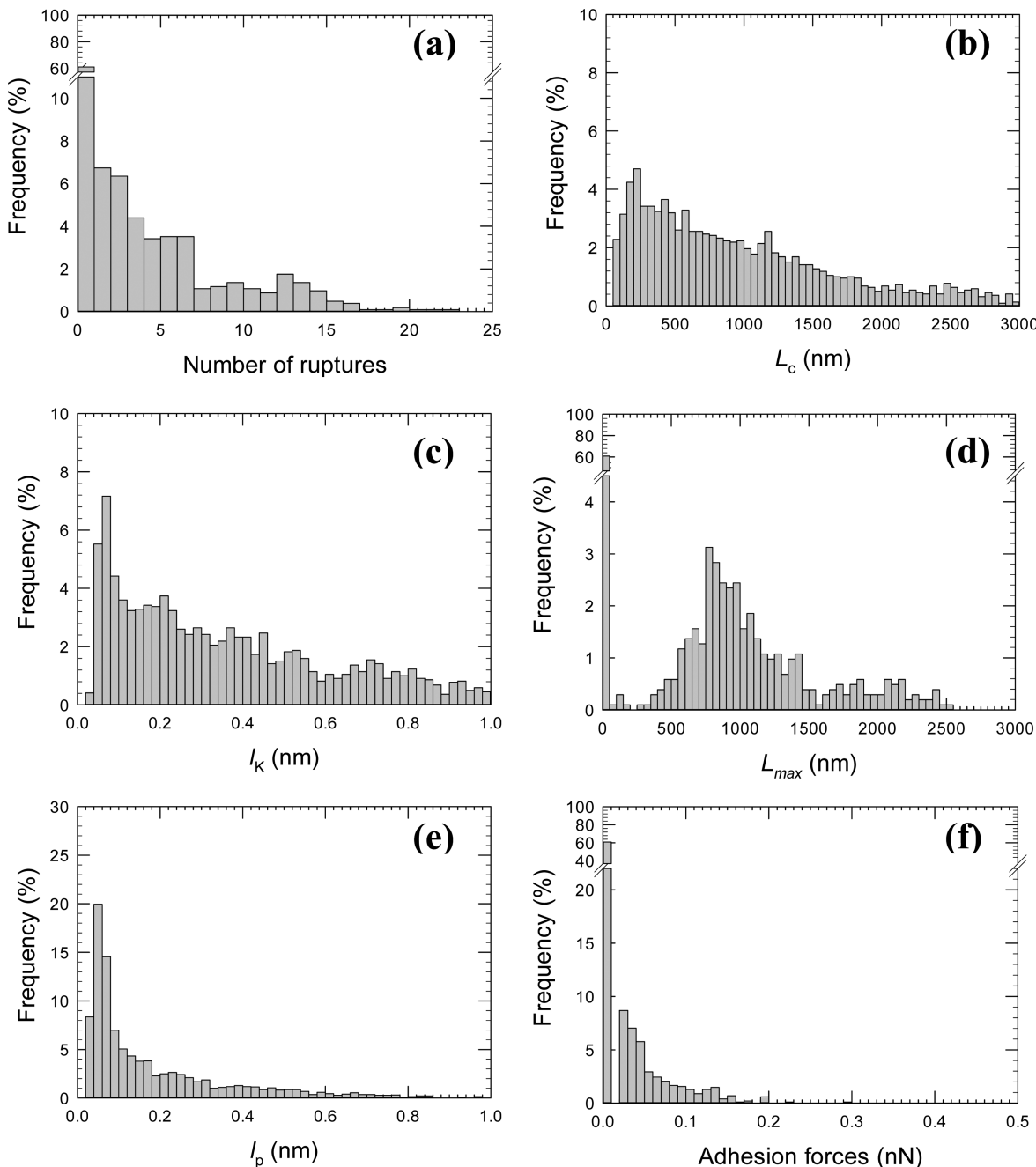


Figure 7. Conformational properties of poly-*N*-acetyl glucosamine-rich EPS of *P. fluorescens* 21 h-old biofilm obtained by single molecule force spectroscopy (SMFS) by using a WGA functionalized AFM tip. Statistical distributions of (a) the number of ruptures, (b) contour length L_c , (c) Kuhn length l_K , (d) the maximum length of the retraction curve L_{max} , (e) persistence length l_p , and (f) the adhesion forces (i.e., the force at the last rupture).

the analysis of experimental force curves with the FJC and WLC models. The present work evaluated, for the first time and *in situ* on a living Pf biofilm, the occurrence of glycogen, galactose, and *N*-acetyl glucosamine-rich EPS. Those EPS presented a high complexity in terms of structure and conformational properties, and seemed to be associated with peptide domains.

■ ASSOCIATED CONTENT

S Supporting Information

Raman spectra of glycogen, galactan, chitin, and 21 h-old biofilm. Statistical distributions of the distance between two

consecutive force ruptures obtained from force–displacement curves. Statistical distributions of the rupture forces obtained from force–displacement curves. Statistical distributions of the number of monomers obtained from force–displacement curves (results from the FJC and WLC models). Examples of retraction force curves performed by SMFS (empty circles) on *P. fluorescens* 21 h-old biofilm on Ge crystal with the Concanavalin A, PAO1, and WGA modified AFM tips, and fitting of force curves with the FJC and WLC theoretical models. Tables with the physical parameters (number of monomers, Kuhn length, contour length, persistence length, and optimization parameter) extracted from the experimental

data. This material is available free of charge via the Internet at <http://pubs.acs.org>.

AUTHOR INFORMATION

Corresponding Author

*E-mail: gregory.francius@univ-lorraine.fr. Phone: (33) 03 83 68 52 36. Fax: (33) 03 83 27 54 44.

Notes

The authors declare no competing financial interest.

REFERENCES

- (1) Flemming, H. C.; Wingender, J. The Biofilm Matrix. *Nat. Rev. Microbiol.* **2010**, *8*, 623–633.
- (2) Merritt, K.; An, Y. Factors Influencing Bacterial Adhesion. In *Handbook of Bacterial Adhesion*; An, Y., Friedman, R., Eds.; Humana Press: Totowa, New Jersey, 2000; pp 53–72.
- (3) Kumar, C. G.; Anand, S. K. Significance of Microbial Biofilms in Food Industry: a Review. *Int. J. Food Microbiol.* **1998**, *42*, 9–27.
- (4) Costerton, J. W.; Lewandowski, Z.; Caldwell, D. E.; Korber, D. R.; Lappin-Scott, H. M. Microbial Biofilms. *Annu. Rev. Microbiol.* **1995**, *49*, 711–745.
- (5) Brown, M. J.; Lester, J. N. Comparison of Bacterial Extracellular Polymer Extraction Methods. *Appl. Environ. Microbiol.* **1980**, *40*, 179–185.
- (6) Froelund, B.; Palmgren, R.; Keiding, K.; Nielsen, P. H. Extraction of Extracellular Polymers from Activated Sludge Using a Cation Exchange Resin. *Water Res.* **1996**, *30*, 1749–1758.
- (7) Yuan, S.-J.; Sun, M.; Sheng, G.-P.; Li, Y.; Li, W.-W.; Yao, R.-S.; Yu, H.-Q. Identification of Key Constituents and Structure of the Extracellular Polymeric Substances Excreted by *Bacillus megaterium* TF10 for Their Flocculation Capacity. *Environ. Sci. Technol.* **2011**, *45*, 1152–1157.
- (8) Beveridge, T. J.; Graham, L. L. Surface-Layers of Bacteria. *Microbiol. Rev.* **1991**, *55*, 684–705.
- (9) Hung, C. C.; Santschi, P. H.; Gillow, J. B. Isolation and Characterization of Extracellular Polysaccharides Produced by *Pseudomonas fluorescens* Biovar II. *Carbohydr. Polym.* **2005**, *61*, 141–147.
- (10) Kives, J.; Orgaz, B.; SanJose, C. Polysaccharide Differences Between Planktonic and Biofilm-Associated EPS from *Pseudomonas fluorescens* B52. *Colloids Surf., B* **2006**, *52*, 123–127.
- (11) Beech, I. B.; Gaylarde, C. C.; Smith, J. J.; Geesey, G. G. Extracellular Polysaccharides from *Desulfovibrio desulfuricans* and *Pseudomonas fluorescens* in the Presence of Mild and Stainless Steel. *Appl. Microbiol. Biotechnol.* **1991**, *35*, 65–71.
- (12) Quilès, F.; Polyakov, P.; Humbert, F.; Francius, G. Production of Extracellular Glycogen by *Pseudomonas fluorescens*: Spectroscopic Evidence and Conformational Analysis by Biomolecular Recognition. *Biomacromolecules* **2012**, *13*, 2118–2127.
- (13) Pink, J.; Smith-Palmer, T.; Chisholm, D.; Beveridge, T. J.; Pink, D. A. An FTIR Study of *Pseudomonas aeruginosa* PAO1 Biofilm Development: Interpretation of ATR-FTIR Data in the 1500–1180 cm⁻¹ Region. *Biofilms* **2005**, *2*, 165–175.
- (14) Quilès, F.; Humbert, F.; Delille, A. Analysis of Changes in Attenuated Total Reflection FTIR Fingerprints of *Pseudomonas fluorescens* from Planktonic State to Nascent Biofilm State. *Spectrochim. Acta, Part A* **2010**, *75*, 610–616.
- (15) Schuster, K. C.; Reese, I.; Urlaub, E.; Gapes, J. R.; Lendl, B. Multidimensional Information on the Chemical Composition of Single Bacterial Cells by Confocal Raman Microspectroscopy. *Anal. Chem.* **2000**, *72*, 5529–5534.
- (16) Huang, W. E.; Griffiths, R. I.; Thompson, I. P.; Bailey, M. J.; Whiteley, A. S. Raman Microscopic Analysis of Single Microbial Cells. *Anal. Chem.* **2004**, *76*, 4452–4458.
- (17) Sandt, C.; Smith-Palmer, T.; Pink, J.; Brennan, L.; Pink, D. Confocal Raman Microspectroscopy as a Tool for Studying the Chemical Heterogeneities of Biofilms *in situ*. *J. Appl. Bacteriol.* **2007**, *103*, 1808–1820.
- (18) Ivleva, N. P.; Wagner, M.; Horn, H.; Niessner, R.; Haisch, C. Towards a Nondestructive Chemical Characterization of Biofilm Matrix by Raman Microscopy. *Anal. Bioanal. Chem.* **2009**, *293*, 197–206.
- (19) Pradhan, N.; Pradhan, S. K.; Nayak, B. B.; Mukherjee, P. S.; Sukla, L. B.; Mishra, B. K. Micro-Raman Analysis and AFM Imaging of *Acidithiobacillus ferrooxidans* Biofilm Grown on Uranium Ore. *Res. Microbiol.* **2008**, *159*, 557–561.
- (20) Malki, M.; Casado, S.; Lopez, M. F.; Caillard, R.; Palomares, F. J.; Gago, J. A. M.; Vaz-Dominguez, C.; Cuesta, A.; Amils, R.; Fernandez, V. M.; Velez, M.; De Lacey, A. L.; Olea, D. Physicochemical Characterization of *Acidiphilum* sp. Biofilms. *ChemPhysChem* **2013**, *14*, 1237–1244.
- (21) Lorite, G. S.; de Souza, A. A.; Neubauer, D.; Mizaikoff, B.; Kranz, C.; Cotta, M. A. On the Role of Extracellular Polymeric Substances during Early Stages of *Xylella fastidiosa* Biofilm Formation. *Colloids Surf., B* **2013**, *102*, 519–525.
- (22) Kamjunke, N.; Spohn, U.; Futing, M.; Wagner, G.; Scharf, E. M.; Sandrock, S.; Zippel, B. Use of Confocal Laser Scanning Microscopy for Biofilm Investigation on Paints under Field Conditions. *Int. Biodeterior. Biodegrad.* **2012**, *69*, 17–22.
- (23) Paulsson, M.; Kober, M.; Freijlarsson, C.; Stollenwerk, M.; Wesslen, B.; Ljungb, A. Adhesion of *Staphylococci* to Chemically-Modified and Native Polymers, and the Influence of PreadSORBED Fibronectin, Vitronectin and Fibrinogen. *Biomaterials* **1993**, *14*, 845–855.
- (24) Razatos, A.; Ong, Y. L.; Sharma, M. M.; Georgiou, G. Molecular Determinants of Bacterial Adhesion Monitored by Atomic Force Microscopy. *Proc. Natl. Acad. Sci. U.S.A.* **1998**, *95*, 11059–11064.
- (25) Zeiger, D. N.; Stafford, C. M.; Cheng, Y.; Leigh, S. D.; Lin-Gibson, S.; Lin, N. J. Effects of Sample Preparation on Bacterial Colonization of Polymers. *Langmuir* **2010**, *26*, 2659–2664.
- (26) Andre, G.; Deghorain, M.; Bron, P. A.; van Swam, I. I.; Kleerebezem, M.; Hols, P.; Dufrêne, Y. F. Fluorescence and Atomic Force Microscopy Imaging of Wall Teichoic Acids in *Lactobacillus plantarum*. *ACS Chem. Biol.* **2011**, *6*, 366–376.
- (27) Wang, C.; Yadavalli, V. K. Investigating Biomolecular Recognition at the Cell Surface using Atomic Force Microscopy. *Micron* **2014**, *60*, 5–17.
- (28) Delille, A.; Quilès, F.; Humbert, F. *In Situ* Monitoring of the Nascent *Pseudomonas fluorescens* Biofilm Response to Variations in the Dissolved Organic Carbon Level in Low-Nutrient Water by Attenuated Total Reflectance-Fourier Transform Infrared Spectroscopy. *Appl. Environ. Microbiol.* **2007**, *73*, 5782–5788.
- (29) Hinterdorfer, P.; Dufrêne, Y. F. Detection and Localization of Single Molecular Recognition Events using Atomic Force Microscopy. *Nat. Methods* **2006**, *3*, 347–355.
- (30) Francius, G.; Alsteens, D.; Dupres, V.; Lebeer, S.; De Keersmaecker, S.; Vanderleyden, J.; Gruber, H. J.; Dufrêne, Y. F. Stretching Polysaccharides on Live Cells using Single Molecule Force Spectroscopy. *Nat. Protoc.* **2009**, *4*, 939–946.
- (31) Janshoff, A.; Neitzert, M.; Oberdoerfer, Y.; Fuchs, H. Force Spectroscopy of Molecular Systems - Single Molecule Spectroscopy of Polymers and Biomolecules. *Angew. Chem., Int. Ed.* **2000**, *39*, 3212–3237.
- (32) Francius, G.; Lebeer, S.; Alsteens, D.; Wildling, L.; Gruber, H. J.; Hols, P.; De Keersmaecker, S.; Vanderleyden, J.; Dufrêne, Y. F. Detection, Localization, and Conformational Analysis of Single Polysaccharide Molecules on Live Bacteria. *ACS Nano* **2008**, *2*, 1921–1929.
- (33) Ortiz, C.; Hadzioannou, G. Entropic Elasticity of Single Polymer Chains of Poly(Methacrylic Acid) Measured by Atomic Force Microscopy. *Macromolecules* **1999**, *32*, 780–787.
- (34) Polyakov, P.; Soussen, C.; Duan, J. B.; Duval, J. F. L.; Brie, D.; Francius, G. Automated Force Volume Image Processing for Biological Samples. *PLoS One* **2011**, *6*, e18887.
- (35) Ambler, R. P. Evolutionary Stability of Cytochrome C-551 in *Pseudomonas aeruginosa* and *Pseudomonas fluorescens* Biotype-C. *Biochem. J.* **1974**, *137*, 3–14.

- (36) Paetzold, R.; Keuntje, M.; Theophile, K.; Mueller, J.; Mielcarek, E.; Ngezahayo, A.; Anders-von Ahlfen, A. *In Situ* Mapping of Nitrifiers and Anammox Bacteria in Microbial Aggregates by Means of Confocal Resonance Raman Microscopy. *J. Microbiol. Methods* **2008**, *72*, 241–248.
- (37) Maquelin, K.; Kirschner, C.; Choo-Smith, L. P.; van den Braak, N.; Endtz, H. P.; Naumann, D.; Puppels, G. J. Identification of Medically Relevant Microorganisms by Vibrational Spectroscopy. *J. Microbiol. Methods* **2002**, *51*, 255–271.
- (38) Huang, W. E.; Bailey, M. J.; Thompson, I. P.; Whiteley, A. S.; Spiers, A. J. Single-Cell Raman Spectral Profiles of *Pseudomonas fluorescens* SBW25 Reflects In Vitro and In Planta Metabolic History. *Microb. Ecol.* **2007**, *53*, 414–425.
- (39) Nivens, D.; Chambers, J. Q.; Anderson, T. R.; Tunlid, A.; Smit, J.; White, D. C. Monitoring Microbial Adhesion and Biofilm Formation by Attenuated Total Reflection/Fourier Transform Infrared Spectroscopy. *J. Microbiol. Methods* **1993**, *17*, 199–213.
- (40) Huang, W. E.; Ude, S.; Spiers, A. J. *Pseudomonas fluorescens* SBW25 Biofilm and Planktonic Cells Have Differentiable Raman Spectral Profiles. *Microb. Ecol.* **2007**, *53*, 471–474.
- (41) Humbert, F.; Quilès, F.; Delille, A. *In Situ* Assessment of Drinking Water Biostability Using Nascent Reference Biofilm ATR-FTIR Fingerprint. In *Current Research Topics in Applied Microbiology and Microbial Biotechnology*; Mendez-Vila, A., Ed.; World Scientific Publishing: Seville, Spain, 2009; pp 268–272.
- (42) Camesano, T. A.; Abu-Lail, N. I. Heterogeneity in Bacterial Surface Polysaccharides, Probed on a Single-Molecule Basis. *Biomacromolecules* **2002**, *3*, 661–667.
- (43) Cui, S.; Yu, Y.; Lin, Z. Modeling Single Chain Elasticity of Single-Stranded DNA: A Comparison of Three Models. *Polymer* **2009**, *50*, 930–935.
- (44) Arce, F. T.; Carlson, R.; Monds, J.; Veeh, R.; Hu, F. Z.; Stewart, P. S.; Lal, R.; Ehrlich, G. D.; Avci, R. Nanoscale Structural and Mechanical Properties of Nontypeable *Haemophilus influenzae* Biofilms. *J. Bacteriol.* **2009**, *191*, 2512–2520.
- (45) Melendez, R.; Melendez-Hevia, E.; Canela, E. I. The Fractal Structure of Glycogen: A Clever Solution to Optimize Cell Metabolism. *Biophys. J.* **1999**, *77*, 1327–1332.
- (46) Kajava, A. V.; Cheng, N.; Cleaver, R.; Kessel, M.; Simon, M. N.; Willery, E.; Jacob-Dubuisson, F.; Locht, C.; Steven, A. C. Beta-Helix Model for the Filamentous Haemagglutinin Adhesin of *Bordetella pertussis* and Related Bacterial Secretory Proteins. *Mol. Microbiol.* **2001**, *42*, 279–292.
- (47) Yoder, M. D.; Keen, N. T.; Jurnak, F. New Domain Motif - The Structure of Pectate Lyase-C, a Secreted Plant Virulence Factor. *Science* **1993**, *260*, 1503–1507.
- (48) Ainavarapu, R. K.; Brujic, J.; Huang, H. H.; Wiita, A. P.; Lu, H.; Li, L. W.; Walther, K. A.; Carrion-Vazquez, M.; Li, H. B.; Fernandez, J. M. Contour Length and Refolding Rate of a Small Protein Controlled by Engineered Disulfide Bonds. *Biophys. J.* **2007**, *92*, 225–233.
- (49) Grater, F.; Heider, P.; Zangi, R.; Berne, B. J. Dissecting Entropic Coiling and Poor Solvent Effects in Protein Collapse. *J. Am. Chem. Soc.* **2008**, *130*, 11578–11579.
- (50) Tobi, D.; Elber, R. Distance-Dependent, Pair Potential for Protein Folding: Results from Linear Optimization. *Proteins: Struct., Funct., Genet.* **2000**, *41*, 40–46.